Marine and Petroleum Geology 150 (2023) 106095

Contents lists available at ScienceDirect

Marine and Petroleum Geology

journal homepage: www.elsevier.com/locate/marpetgeo

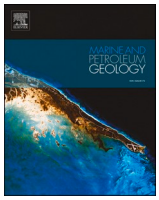

Complex flow in tight oil reservoirs: A new perspective

Shuheng Du [a,b,c,*], Jun Jin [d], Yongmin Shi [a], Fuqiang Sun [e]

[a] School of Earth and Space Sciences, Peking University, Beijing, 100871, China
[b] State Key Laboratory of Nonlinear Mechanics, Institute of Mechanics, Chinese Academy of Sciences, Beijing, 100190, China
[c] School of Engineering Science, University of Chinese Academy of Sciences, Beijing, 100049, China
[d] Research Institute of Exploration and Development, Xinjiang Oilfield Company, Karamay, 834000, China
[e] The University of Hong Kong, Hong Kong, 999077, China

ARTICLE INFO

Keywords:
Tight oil
Fluid transport
Minerals
Mechanical properties
Flow

ABSTRACT

This study aimed to investigate a new mechanism of complex flow in tight oil reservoirs impacted by heterogeneous minerals. In this study, a new classification scheme for seepage channels based on mineral types was firstly developed after considering the differences in their mechanical properties. There are nine types of seepage channels, consisting of four types of main minerals or mineral combinations. Results showed that the maximum flow velocity increases in a non–linear way as the average diameter of each type of seepage channel increases. Thus, the larger the diameter of the space, the greater the potential flow capability. As the injection pressure increases, the flow velocity could be higher in the larger seepage channels than the smaller seepage channels. When the oilfield enters the middle and later periods, in general, the oil in most of the large spaces has been removed. The average flow velocity (the comprehensive potential flow capability) has almost no relationship with the type of space; thus, a small space does not have a greater potential of exploitation than a large space. This conclusion points to a new direction for enhancing unconventional oil recovery.

1. Introduction

The exploration and development of oil, natural gas and new energy involves geology, mechanics, physics, chemistry and many other disciplines, which is directly related to the survival and development of human society (Zhao, 2018; Eremin et al., 2020; Geng, 2020; ; Cai et al., 2022; Hematpur et al., 2023).

The continental sandstone reservoir in China is distinctive because of its special sedimentary and structural characteristics (Ge et al., 2015, 2017; Jiang et al., 2016; Cao et al., 2016a; 2016b; Wang et al., 2016a). Generally, the minerals in a sandstone reservoir consist of quartz, feldspar, rock debris, and various clay minerals, such as kaolinite (Alexandre, 2009). According to the principle of sedimentology, the formation of seepage channels are essentially the result of the accumulation, compaction, and subsequent diagenesis of minerals, and it is formed by the primary and secondary boundaries of minerals; moreover, the boundaries of the seepage channels are the mineral boundaries after denudation, transportation, and reconstruction (Salem, 2005; Macquaker et al., 2014; Alarji et al., 2022). The characteristics of seepage channels largely reflect the sorting and grinding properties of the particles, which is a true reflection of the results of deposition, compaction, and modification (Sakran et al., 2015; Du et al., 2019a, 2020, 2019b). Thus, the formation of the seepage channels and minerals during the deposition process is symbiotic: without minerals, there are no seepage channels (Sakran et al., 2016). There is still much uncertainty about the relationship between the flowing path, at the microscopic level, and the combination of different seepage channels formed by different minerals (Hu et al., 2016 and 2017; Ju et al., 2017; Du et al., 2018a and 2018b).

Due to concerns about the flow mechanism in a sandstone reservoir, many published studies have investigated the physical simulation of the flow path in a reservoir and some of them obtained qualitative results (Hou et al., 2015; Sakran et al., 2015 and 2016). However, the findings could not be analyzed using quantitative methods (Zhang et al., 2013; Hu et al., 2013; Zhu et al., 2022). Although some studies used nuclear magnetic resonance (NMR) technology to quantitatively determine the flow velocity distribution at different times and locate the liquid, the location could simply be inverted by the relaxation time and it was not possible to identify the liquid's real location by sight (Xu et al., 2011). Some researchers think that the relaxation time could not precisely reflect the type of the space (Pia et al., 2016; Peng et al., 2011; Wang et al., 2016b). Few previous studies have investigated the flow path and the flow velocity distribution, and their relationship with the minerals

* Corresponding author. School of Earth and Space Sciences, Peking University, Beijing, 100871, China.
E-mail address: dushuheng@imech.ac.cn (S. Du).

https://doi.org/10.1016/j.marpetgeo.2023.106095
Received 10 October 2022; Received in revised form 9 December 2022; Accepted 2 January 2023
Available online 11 January 2023

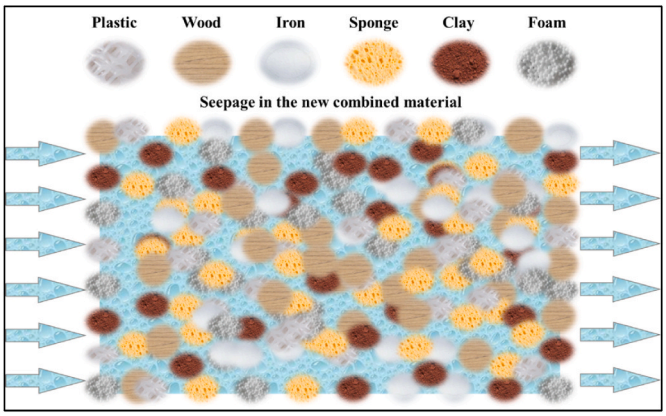

Fig. 1. Flow process in the new combined material. The new material is used to illustrate the basis of and necessity for seepage channels reclassification in a tight oil reservoir. The rectangular combined material is filled with small materials such as plastic, wood, iron, sponge, clay and foam and these small materials are packed randomly. The blue arrow on the left and right indicates the fluid injection gate and the outflow gate. As the properties in mechanics and other aspects of all the small materials are varied, the flow process would also varied in different seepage channels related to different small materials such as the wood–plastic, foam–clay, iron–plastic and so on. The small materials are used to compare with the different types of materials in a tight oil reservoir and the combined material indicates the actual tight oil reservoir. This analogy would help to make sense.

(Markevich and Ceil, 1991; Nishank et al., 2017).

As we can see, case studies of the microscopic seepage channels have presented a detailed analysis of the flow path in the oil and gas reservoir (Zhang et al., 2013; Sakran et al., 2015 and 2016). Recently, simpler and more rapid tests and description methods have been developed to investigate the microscopic seepage channels, including, "Laser Scanning Confocal Microscope" (LSCM), "Focus Ion Beam–Scanning Electron Microscope" (FIB–SEM), "Micro–Computed Tomography" (Micro–CT), and "Nano–Computed Tomography" (Nano–CT) (Hu et al., 2013; Hou et al., 2015). However, most of the classification methods used to study seepage channels focus on its size and external shape so little attention has been paid to the minerals in these seepage channels. Therefore, a method to classify the seepage channels should be developed, and the impact should be quantified (Macquaker et al., 2014; Sakran et al., 2015).

Besides, some scholars have used fractal theory to study the complex distribution characteristics of seepage channels (Zhao et al., 2019; Vinoth et al., 2020; Tan et al., 2020). Obviously, the flow path of the fluids in the seepage channels would be more likely to be described by this theory, but previous studies have not addressed this issue (Nittman, 1985; Krohnce, 1988; Huang et al., 2017). Most researchers have only focused on describing the shape of the flow path, such as a finger–like or a cone–shaped path (Macquaker et al., 2014; Sakran et al., 2015).

In addition, some scholars have also discussed the influence of mineral wettability on flow characteristics. Most of them analyzed the lattice characteristics, chemical composition, reaction between injected fluid and minerals from the perspective of mineral chemistry, so as to explore the influence of those factors on the flow characteristics, including the phenomena of water sensitivity, salt sensitivity, acid sensitivity and so on. Such as Ju et al. (2017) believed that the fraction of mineral surfaces containing roughness pits filled with brine may be the most important reservoir characteristic that controls wettability in sandstone. Kang et al. (2019) discovered the reaction mechanisms between coal samples and hydrogen peroxide and the mechanisms to improve the flow capacity of coal reservoirs were analyzed. In fact, in this process, the minerals in the coal seam dissolved and the wettability of the pore surface changed. Yuan (2020) found that the structural characteristics and relative content differences of micropores in the samples are the internal mechanism of the difference of water sensitivity effect types. Some scholars have also studied the use of wettability reversal in the flow process to improve oil recovery. Like the multi-component ion exchange, MIE, at the clay surface (Lager et al., 2007), expansion of the ionic double-layer at the rock surface (Ligthelm et al., 2009) and so on. Based on this, Strand et al. (2016) presented the crucial wetting parameters for the different phases, oil, brine and rock and discussed the symbiotic interaction between the different wetting parameters on the initial wetting properties. All of these are beneficial to the mechanism exploration of minerals on flow, but more reservoir spaces are mostly formed by mineral combinations, so further research is needed.

As to the former researches, though many scholars have studied the flow path in various reservoirs; however, to date, little attention has been paid to the respective flow characteristics in different types of spaces and the similarities and differences between these flow characteristics. So the quantitative differences in the flow process for the channels formed by different minerals in tight reservoirs have not been solved.

To conclude, the main innovation of this study is that discovering and characterizing the uncertainty about the relationship between the flowing paths formed by the combination of different seepage channels formed by different minerals at the microscopic level quantitatively. The final innovation point would be that we get the mechanism of the differences in the flow process for seepage channels formed by different minerals in a tight reservoir via the combination of three main factors in reservoir which consists of minerals, pore-throat and fluid.

It is important to investigate the new mechanism of the complex flow in tight oil reservoirs impacted by heterogeneous minerals. The new mechanism could be a practical tool to understand flow pattern in tight-oil reservoirs. It will answer the key question which is for the rocks after water flooding, the remaining oil specifically exists in the pores or fractures formed by the boundaries of which types of minerals. Then engineers could select reasonable displacement materials and formulate reasonable development means to achieve efficient recovery of remaining oil in tight oil rocks.

2. Methodology

2.1. Basis and necessity for seepage channels reclassification

Obviously, the core issue of this study is the differences in the seepage channels formed by different minerals and the necessity of redefining the types of seepage channels based on mineral types.

In the process of tight oil exploitation, the fluids will generate different levels of shear stress and normal stress on the boundaries of the different seepage channels formed by different minerals. Thus, the mineral surface in contact with the fluids will exhibit different degrees of elastic deformation due to differences in the mechanical properties (including Young's modulus, Poisson's ratio) of the minerals, which will lead to determining the differences in the flow characteristics of all the seepage channels (Nittman, 1985; Krohnce, 1988; Huang et al., 2017).

In fact, different rock materials, similar to some non-geological materials, have the characteristics of elasticity or plasticity when subjected to external forces. Therefore, from the perspective of elastic deformation in materials, the properties of the combination of elastic and non-geological materials are similar to those of rock materials, which can be analogized. In this way, we can find new ways to solve the problem. (Zeng et al., 2020; Jiang et al., 2016). In order to illustrate the necessity for seepage channels reclassification, we could construct a type of combined material including the iron, foam, sponge, wood, clay and plastic with different sizes and shapes (Fig. 1). Thus, the combined material would contain the seepage channels formed by different materials, such as iron–wood, clay– plastic, foam–sponge, and so on. When we inject fluid with unsteady velocity into it, the fluid velocity will change in different degrees along with the flow in different channels.

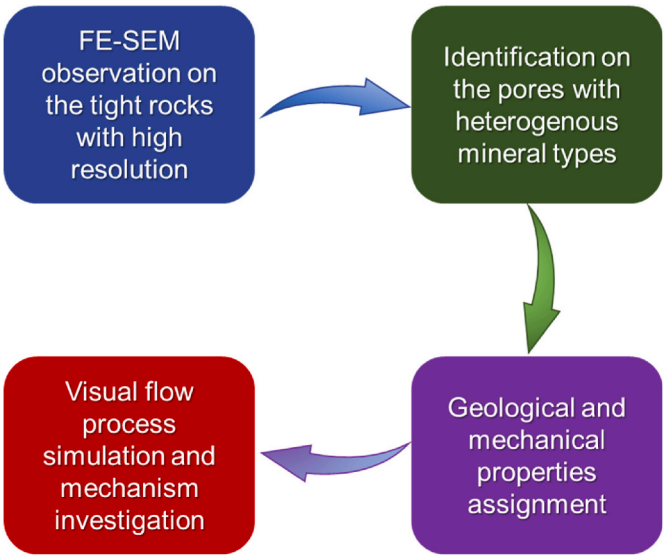

Fig. 2. Technical process of the visual flow simulation. The FE–SEM observation could offer the clear images of the tight oil reservoir with high resolution. The minerals are identified with the help of the Energy Dispersive Spectroscopy (EDS). EDS technology could get the quantitative data of the element distribution, the final mineral type could be determined based on the element analysis of professional software. The basis mechanical assignment and the visual flow would be shown in the text.

Table 1
Characteristics in geophysics and mechanics of minerals. The properties of four main minerals are listed. The clay minerals mainly consists of kaolinite, illite and montmorillonite. This table would be the basis of the mechanical assignment in the flow simulation.

Type of minerals	V_p/ m/s	V_s/ m/s	Density/g/ cm^3	Young's modulus/GPa	Poisson Ratio
Quartz	6000	4035	2.65	93.81	0.09
Feldspar	6060	3350	2.63	75.56	0.28
Clay minerals	3000	1800	2.20	17.37	0.22
Black mica	5810	3360	2.82	79.51	0.25

The main reason is that the mechanical properties of the boundary in each type of seepage channel are different, so the boundaries would have different degrees of micro–deformation, resulting in different energy losses (Benito et al., 2005; Babiak et al., 2018; Cabalar et al., 2018; Mathew et al., 2018; Tozzi et al., 2018).

Similarly, we can find the same phenomenon from nature. When we see the stream flowing in the mountains, it passes through a lot of rocks, but different rocks have different lithology and forming conditions, resulting in different mechanical properties (Gran and Paola, 2001; Stokes et al., 2009; Gula et al., 2015), so the velocity will be affected to varying degrees. Actually, we can compare the rocks with different properties in the mountains to different types of mineral particles in the reservoir, and compare the streams to the fluids in the reservoir. Therefore, when the fluid passes through the reservoir space formed by different mineral combinations in the reservoir, the flow velocity may also be different. This type of difference is the very object of quantitative research. So the seepage channels need to be reclassified based on the type of pore minerals.

2.2. Technical process of flow simulation

The technical process of the visual flow simulation is shown in Fig. 2. Since each single mineral has its own geophysical and mechanical characteristics, the impacts on the microscopic flow path caused by each mineral or the combination of minerals would also vary, which could be a distinctive aspect of the seepage channels.

When investigating the grids associated with the minerals and

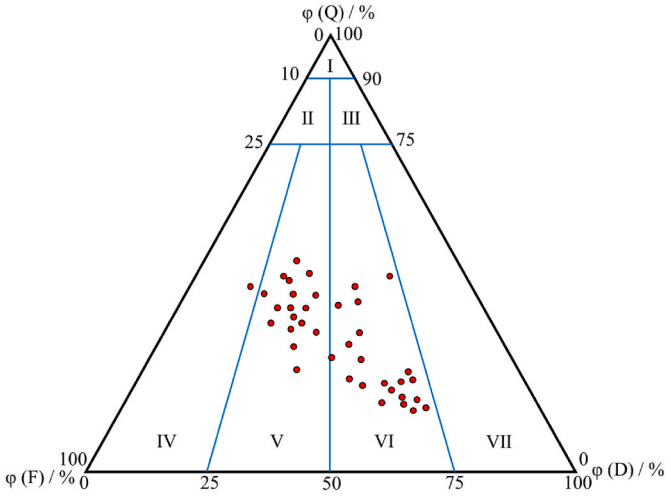

Fig. 4. Lithologic classification map of tight oil reservoir in Yanchang formation, Ordos Basin. The three angles in the equilateral triangle represent three typical main mineral types in sandstone, "Q" represents "quartz", "F" represents feldspar and "D" represents debris. The numerical range of the three sides represents the content of quartz, feldspar and debris from 0 to 100%, respectively. Arabic numerals "I", "II", "III", "IV", "V", "VI", "VI" and "VII" represent seven kinds of sandstone lithology, including quartz sandstone, feldspathic quartz sandstone, lithic quartz sandstone, feldspathic sandstone, lithic arkose, feldspathic lithic sandstone and lithic sandstone. The red data points marked in the figure represent different samples. Except that a small part of the data are quoted from Guo et al. (2013), the rest are the supplementary experimental samples in this study. According to the content of three minerals in each sample, its position is determined. Thus, the lithologic distribution of Yanchang Formation reservoir can be clearly obtained.

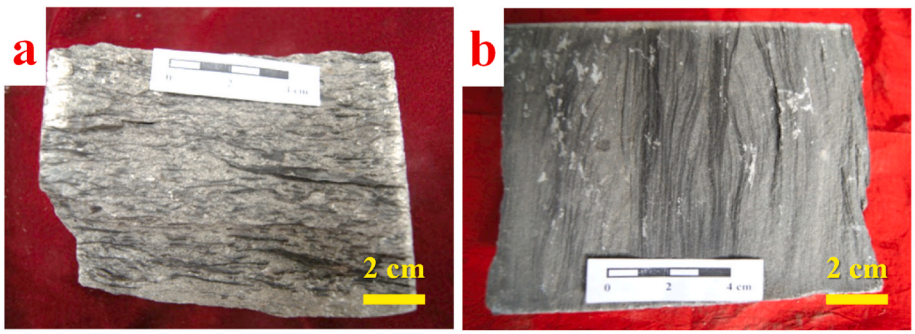

Fig. 3. Tight oil reservoir cores of Yanchang Formation in Ordos Basin (Samples a and b are taken from different depths of the same well).

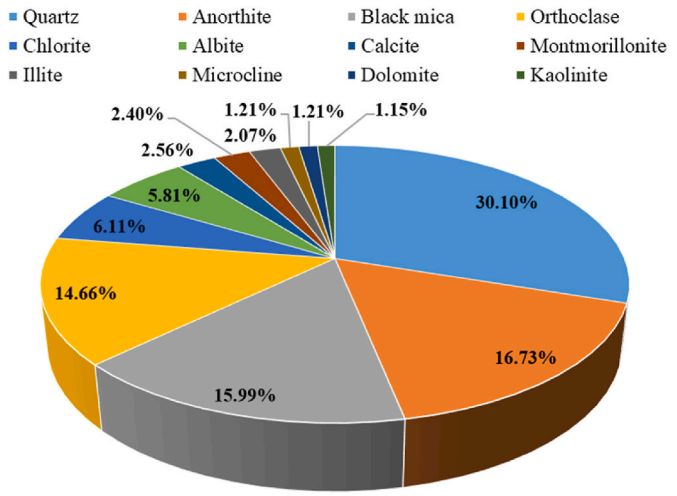

Fig. 5. Mineral analysis results of X-ray diffraction of Yanchang Formation reservoir. By comparing the X-ray diffraction patterns of samples with the typical standard patterns of minerals, different types of minerals are identified. The different colors in the figure represent different kinds of minerals, and the numbers represent the average content of each mineral in the reservoir.

Table 2
Test results of physical properties of tight oil reservoir in Yanchang formation.

Sample \Properties	Porosity/ %	Permeability/ $10^{-3}\mu m^2$	Throat radius corresponding to peak permeability/μm	Efficiency of mercury withdrawal/%
A	2.0	0.005	0.16	52.3
B	9.4	0.068	0.4	29.1
C	8.6	0.089	0.63	38.3
D	10.4	0.038	0.16	22.1
E	14.8	0.289	0.63	43.0
F	7.9	0.032	0.4	26.5
G	13.1	0.046	4	24.4
H	15.2	0.356	1	26.8
I	14.9	0.608	1	38.1
K	6.2	0.041	0.63	34.3

seepage channels, porosity and permeability must be addressed.

As the minerals in seepage channels are solid, their porosity value would be set to "0" and the porosity of value of the seepage channels would be set to "100%". Similarly, the permeability value of the minerals would be set to "0"; the permeability values of the seepage channels were assigned based on the Poiseuille equation.

As to the mechanical properties assignment of minerals, the geophysical and mechanical characteristics of these minerals, such as the P–wave velocity (V_P), the S–wave velocity (V_s), the density, Young's modulus, and the Poisson's ratio were also listed in Table 1.

Among them, P-wave velocity and S-wave velocity could be obtained through the relevant literature (Ahrens, 1995; Wan et al., 2020). Young's modulus could be calculated by the formula consists of three parameters: P-wave velocity, S-wave velocity and density. Poisson's ratio could be calculated by the formula consists of two parameters: P-wave velocity, S-wave velocity (Du et al., 2015, 2016). The equations are as follows:

$$E = \rho v_s^2 \frac{3v_p^2 - 4v_s^2}{v_p^2 - v_s^2} \tag{1}$$

$$\mu = \frac{0.5v_p^2 - v_s^2}{v_p^2 - v_s^2} \tag{2}$$

In equations (1) and (2), "E" and "μ" represent the Young's modulus and Poisson's ratio of minerals respectively, "ρ" represents the mineral density, and "v_p" and "v_s" represent the P-wave velocity and S-wave velocity of minerals respectively.

Taking quartz as an example, the order of magnitude of mineral boundary deformation rate caused by fluid is roughly estimated. Assuming that both boundaries of a single seepage channel are composed of quartz particles, the particle size of quartz is set as 200 μ m. The fluid pressure is 10 MPa. According to the definition of Young's modulus, the fluid may cause the deformation rate of a single boundary to be about one ten thousandth (about 20 nm). This value is obviously not negligible for tight oil reservoirs with micro-nano pores.

It should be pointed out that the absolute values of wave velocity of some minerals are still not uniform. In order to solve this problem, some minerals parameters were averaged of approximated in this paper to ensure that the relative values of mechanical parameters of each mineral are not confused logically. It means that the value sequence should be fit to the mature conclusion nowadays so that the simulation results would not produce self-contradictory results. The absolute values would be updated in the future study step by step.

It is widely known that reservoir rock is a porous medium and a visco–plasto–elastomer. The viscidity is contributed by the liquid in the space while the elastic–plastic is contributed by the skeleton and the inter–fillings (Antoine et al., 2018; Arash et al., 2019; Nurudeen et al., 2018). In the process of displacement, when the liquid flows inside the space, pressure is applied to the internal boundaries of the seepage channels. The seepage channels would inevitably open and close in this process. Thus, to a certain extent, the microscopic flow process in the reservoir could be treated as a small–scale steady fracturing process without adding sand.

In this study, the visual simulation was done using Wingohfer, a large simulation system of the Core Laboratories. In the simulation, we adopted the principle of pipe flow and flow consistency, which could make the results more believable. In fluid mechanics, the objective is to ensure that the fluid flows in the tubes. In flow mechanics, the objective is to ensure that the fluid flows in the porous media. These two flow laws are described as Poiseuille's law (Li and Zhang, 2007) and Darcy's law (Li, 2015) respectively. The associated equations (3)–(5) are:

$$q = \frac{nA\pi r^4 \Delta p}{8\mu\tau\Delta L} \tag{3}$$

$$q = \frac{AK\Delta p}{\mu\Delta L} \tag{4}$$

Then, based on the extension form of Poiseuille equation, we can obtain the permeability K from equation (5) as followings:

$$q = \frac{n\pi r^4}{8\tau} \tag{5}$$

In equations (3)–(5), q, n, A, r, p, μ, K, L indicate fluid volume per unit time, area density of capillary, cross section area of capillary, capillary radius, pressure difference at both ends, fluid viscosity, permeability, straight length of capillary, respectively.

When we put the Poiseuille equation into the Darcy's law equation, we obtain the Poiseuille's law equation. The porous media consist of bundles of tubes, so the flow in porous media also flows through pipes; thus, the flow in the tubes should be the same as the flow in porous media. In this study, we divided the space of the pore–fracture media into a large number of grids, and we treated the flow in each grid as if it was flowing in a small pipe. Thus, the combination of the pipe flow and flow became one of the most important theoretical bases of this study.

3. Results

3.1. Petrological, mineralogical, and physical characteristics

As the lithology of Yanchang Formation reservoir is tight sandstone,

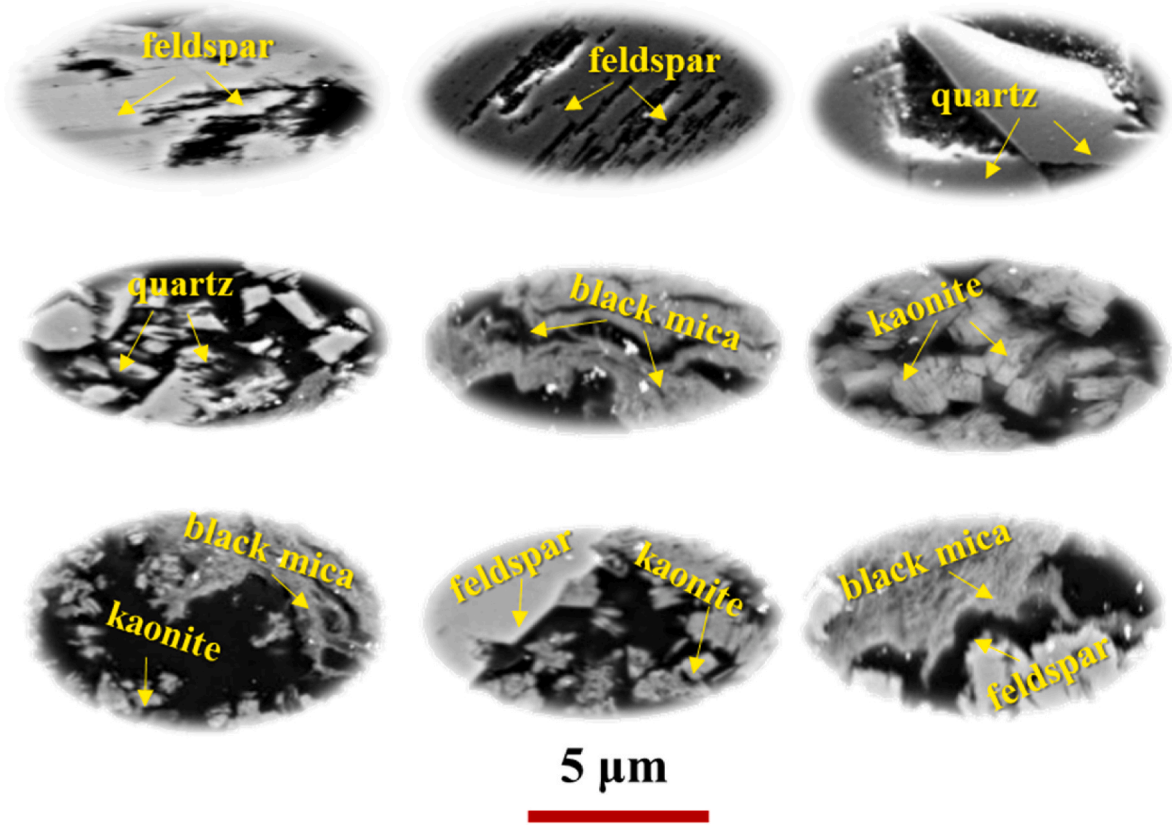

Fig. 6. Minerals identification for the Seepage channels in the tight oil reservoir. The yellow arrows indicate the location of the different minerals. The white indicates the seepage channels formed by these minerals. These images are all real images of tight oil reservoirs of Yanchang formation captured under the FE–SEM.

Table 3
Reclassification Results for the Seepage channels. The first column indicates the label of the seepage channels; The second column indicates the name of the seepage channels; The third column indicates all the minerals which are related to the seepage channel; The fourth column indicates the formation mechanism of these seepage channels; The fifth column indicates the short name of these seepage channels used in this study conveniently; The fifth column indicates the short name of these seepage channels used in this study conveniently; The typical images of these seepage channels has been shown in Fig. 6.

Label	Seepage channels	Relative minerals	Formation mechanism	Abbreviation
1	Corrosional pore inside the feldspar	Feldspar	Corrosion	FCP
2	Corrosional fracture inside the feldspar	Feldspar	Corrosion	FCF
3	Accumulational pore by the feldspar broken	Feldspar	Accumulation	FAP
4	Accumulational pore by the quartz broken	Quartz	Accumulation	QAP
5	Fracture inside the mica cleavage	Mica	Cleavage	MCF
6	Accumulational pore of the interstitial fillings	The interstitial fillings	Accumulation	IAP
7	Accumulational pore of the interstitial fillings-mica	The interstitial fillings and mica	Accumulation	IMAP
8	Accumulational pore of the interstitial fillings-feldspar	The interstitial fillings and feldspar	Accumulation	IFAP
9	Accumulational pore of mica-feldspar	Mica and feldspar	Accumulation	MFAP

the triangle recognition chart composed of quartz, feldspar and debris is used to identify and classify the lithology (Xu, 2017).

Fig. 3 shows the typical core photos of Yanchang Formation reservoir. Fig. 4 shows that the reservoirs are mainly feldspathic lithic sandstone and lithic feldspathic sandstone, and a few of them are feldspathic sandstone. Clastic compositions are mainly feldspar, quartz, rock debris and black mica, with a small amount of heavy minerals. In general, it is characterized by low component maturity and high structural maturity.

As the research object of this paper is the mineral types and the composition of the reservoir space, it will be helpful for us to have an overall grasp of the development of various types of pores by making clear the specific mineral types contained in the reservoir and quantifying them. At the same time, it can also provide the theoretical basis for the study of this paper.

Through a series of X-ray diffraction experiments, it can be concluded that the clastic particles in Yanchang formation are mainly quartz, feldspar, rock debris and black mica (Fig. 5). Quartz accounts for about 30.1% of the total, and feldspar includes calcium feldspar, potassium feldspar, albite, microcline and other types, accounting for about 38.4% of the total. Clay mineral compositions include chlorite, montmorillonite, illite and kaolinite, accounting for about 11.7%. Due to the different content and mechanical properties of minerals, the contents of the reservoir space related to these minerals would also be different, and the flow characteristics of the injected fluid with a certain pressure passing through these pores would also varied. It is necessary to carry out further research.

The porosity, permeability and other physical properties of tight oil reservoir samples of Yanchang Formation were tested. It can be seen from Table 2 that the porosity value ranges from 2.0% to 15.2%, with an average of 10.2%. Permeability value ranges from $0.005 \times 10^{-3}\mu m^2$ to $0.608 \times 10^{-3}\mu m^2$, with an average of $0.157 \times 10^{-3}\mu m^2$. The pore-throat

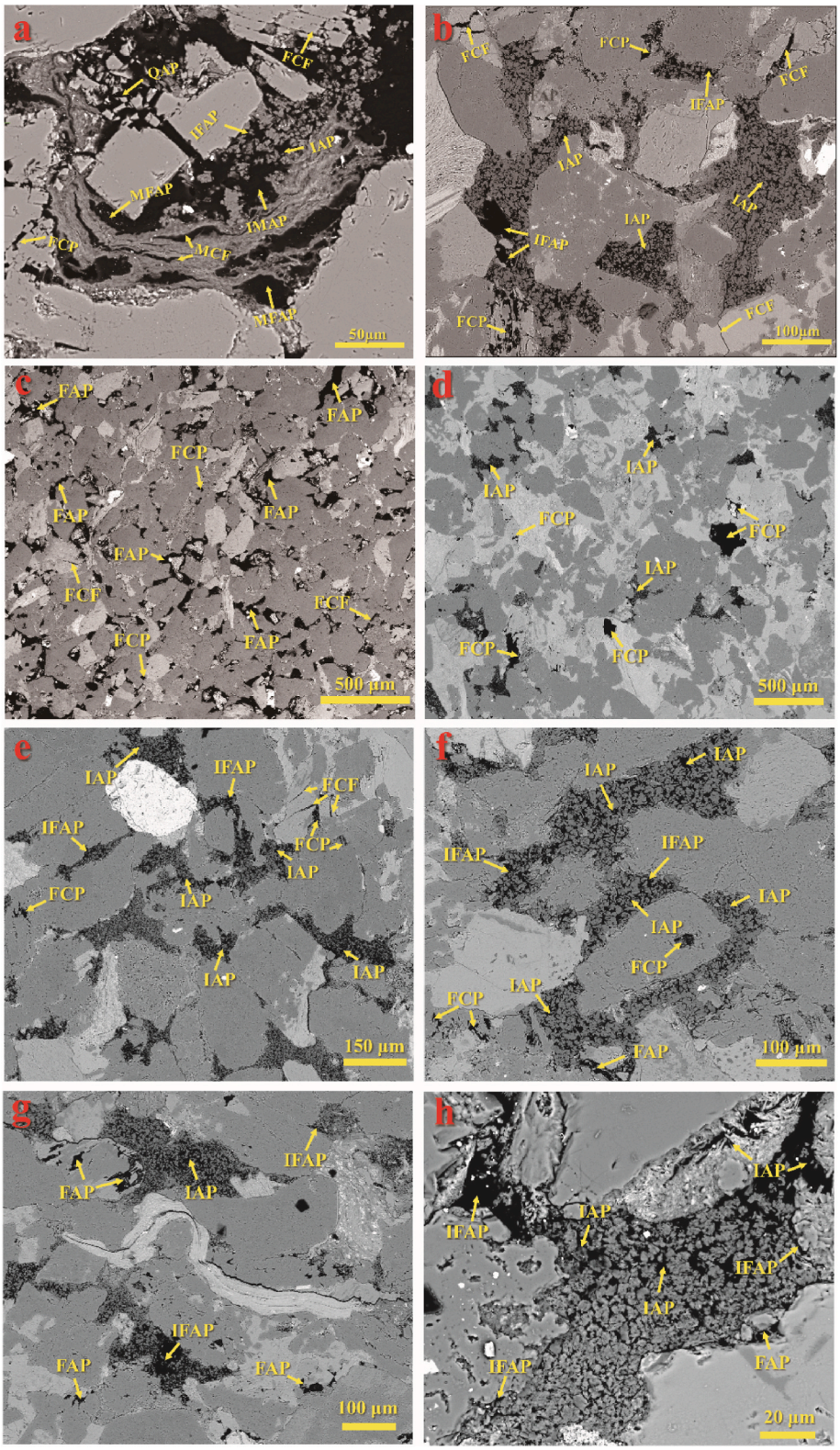

Fig. 7. Identification of the nine seepage channels in the real images of tight oil reservoir of Yanchang formation captured by FE–SEM. All these seepage channels are easily found in the reservoir which would prove the necessity of the differences of flow in them.

radius corresponding to the peak permeability ranges from 0.16 μm to 4 μm, with an average of 0.9 μm. This shows that the pore-throats with the radius value between 0.16 μm and 4 μm are the dominant factor affecting the seepage capacity of Yanchang Formation in this study. The relationships between pore throats and minerals need to be studied urgently. In addition, the efficiency of mercury withdrawal ranges from 22.1% to 52.3%, with an average of 33.5%. As the efficiency of mercury withdrawal can roughly represent the level of oil recovery, above result indicates that the recovery efficiency of the reservoir needs to be further improved, but the location of the remaining oil still needs to be further

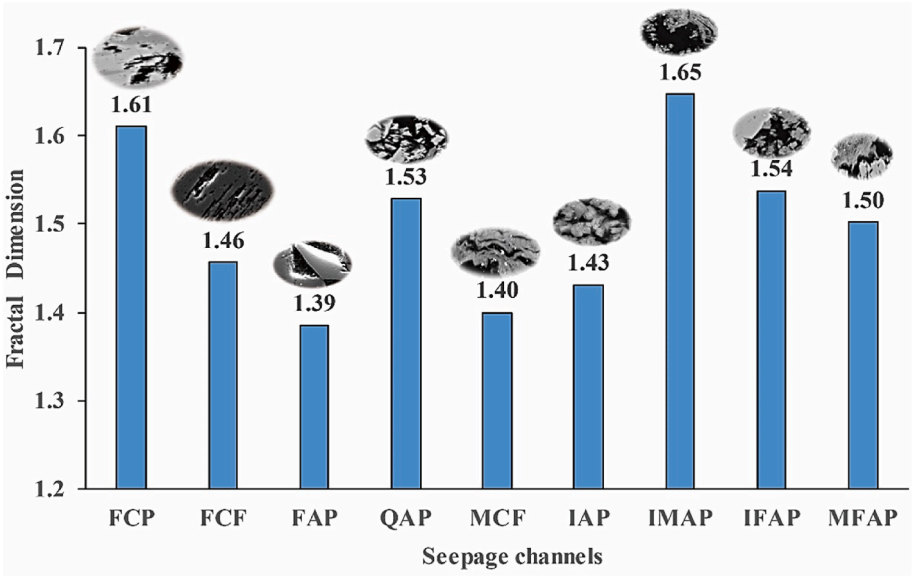

Fig. 8. Fractal dimension calculation of all types of seepage channels. The images of each type of seepage channels are shown in the column respectively.

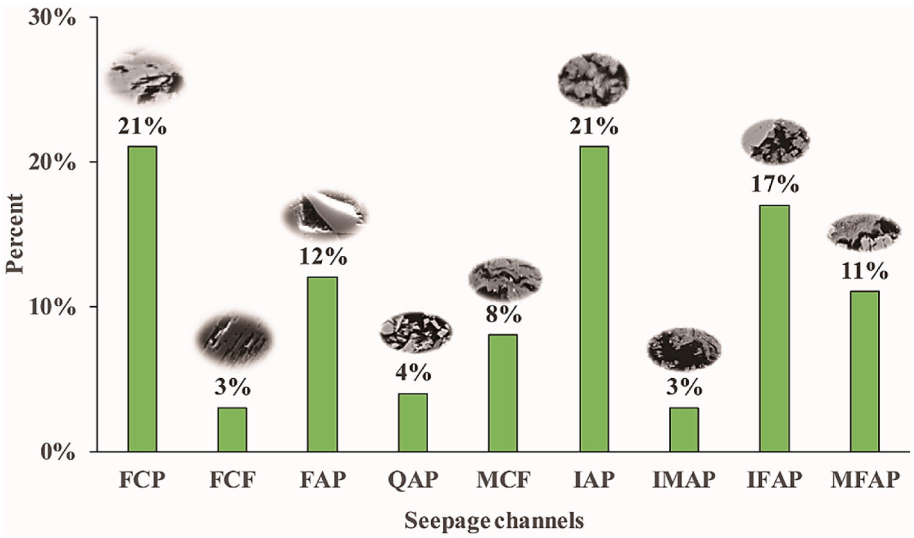

Fig. 9. Content calculation of all types of seepage channels. The images of each type of seepage channels are shown in the column respectively.

studied in combination with minerals.

3.2. Reclassification results for the seepage channels

Scanning electron microscopy (SEM) was used to observe the properties of the minerals in the reservoir at a large–scale level.

From the description presented in the previous section, and after considering the combination of minerals, the mechanism of formation, and the expected differences in the flow process between the fracture and the pore, a new seepage channels classification scheme was developed based on mineral types after considering the differences in their mechanical properties (Fig. 6 and Table 3). As shown in Fig. 6, we could easily find the 4 types of main minerals include feldspar, quartz, black mica, and interstitial fillings.

Interstitial fillings mainly consists of kaolinite, illite and montmorillonite. These minerals would form different seepage channels due to the process of accumulation, dissolution.

This new classification scheme was used to investigate on how the mechanical properties of the minerals affect tight oil exploitation (Fig. 6). Meanwhile, a large amount of image data is the key to improve the reliability of identification results (Wang, 2021; Xu et al., 2021). Since machine learning has been used to process massive data of various disciplines, it should also be used in efficient identification of minerals and pores in the future (Liang and Jia, 2022; Liu et al., 2022; Zhu et al., 2022).

It should be pointed out that porosity and permeability all depend on the sedimentary process obviously. And the formation of seepage channels would be also influenced by the process of sedimentation, compaction, diagenesis and other factors. With the process of particle transport, the degree of mineral roundness will gradually become better, which is conducive to form the seepage channels with smooth mineral boundaries and reduces the energy loss in the flow process. In addition, with the frequent changes of hydrodynamic conditions, the sorting degree of particles will also fluctuate, which will undoubtedly increase the complexity and uncertainty of the seepage channels. Due to the randomness of mineral accumulation and diagenesis, the nine types of seepage channels mentioned above all have their own development probability.

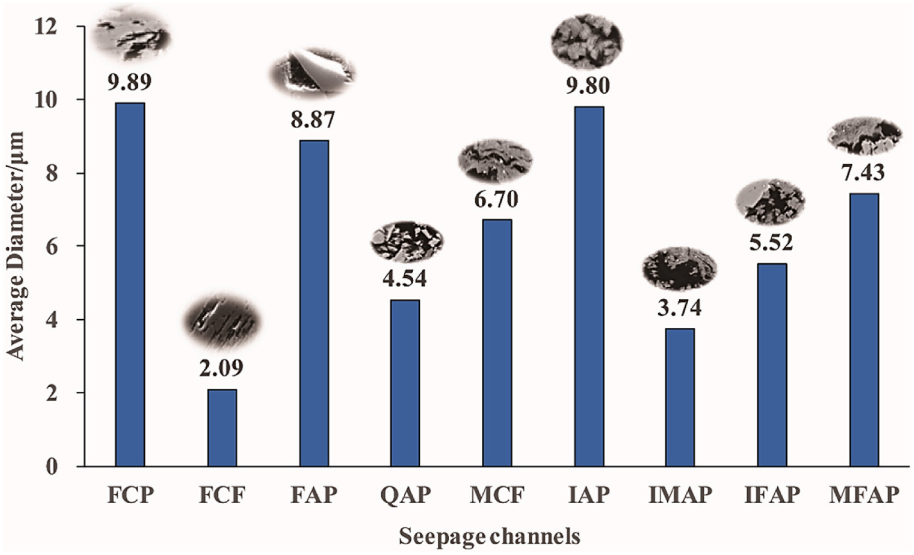

Fig. 10. Average diameter calculation of all types of seepage channels. The images of each type of seepage channels are shown in the column respectively.

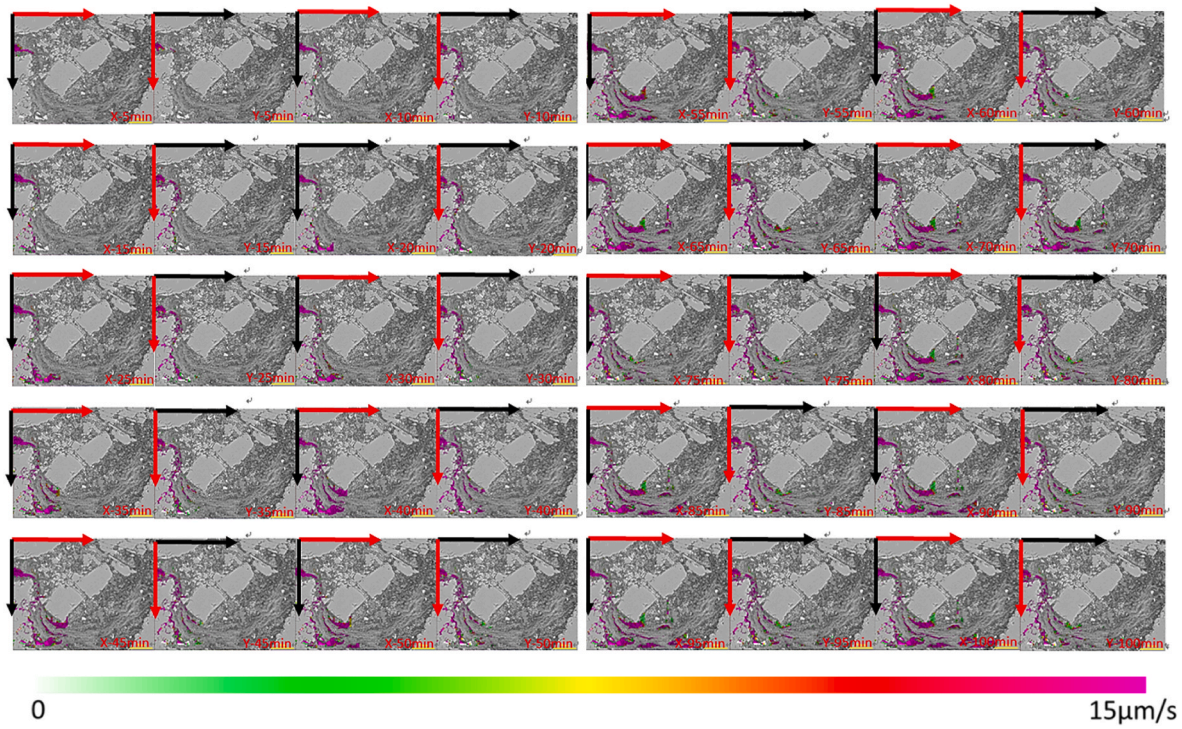

Fig. 11. Visual flow simulation of tight oil exploitation (0–100min). The color of the fluid represents the size of the flow rate, from green, yellow, orange, and red to purple, and the flow rate increases in turn. As to the flow process at a certain time, the authors decompose the velocity into X–velocity (horizontal velocity) and Y–velocity (vertical velocity), expressing the flow characteristics at a certain time with two images in order to make better sense.

After the SEM observation of rock slices, the fractal dimension, the content and the average diameters of each type of seepage channel were computed (Fig. 7 ~10). It should also be noted that due to the sample quality, imaging resolution and element testing accuracy in this study, there is no completely reliable evidence to show that the minerals marked as "black mica" in Figs. 6 and 7 are indeed real black mica. In order to ensure that the simulation can be carried out smoothly, it is marked as "black mica" here to explore the impact of mineral diversity on seepage. Meanwhile, the focus of this study is to provide a new perspective on the study of flow in tight rocks, the identification accuracy of some minerals is not taken as a key concern here. However, when doing similar simulation in the future, more precise experimental instruments can be used to explore the mineral types in more detail.

Previous studies have shown fractal dimension is a quantitative parameter to describe the fractal phenomenon, the fractal characteristics of the pore structure in reservoir rock is obvious, and the fractal dimension could be used to describe the complexity of pore structure quantitatively. Box counting method could be used to calculate the fractal dimension in this study (Mandelbrot, 1967, 1974). The calculation principle is as follows:

$$F = \lim_{r \to \infty} \frac{\ln(N_r)}{\ln(r)} \tag{6}$$

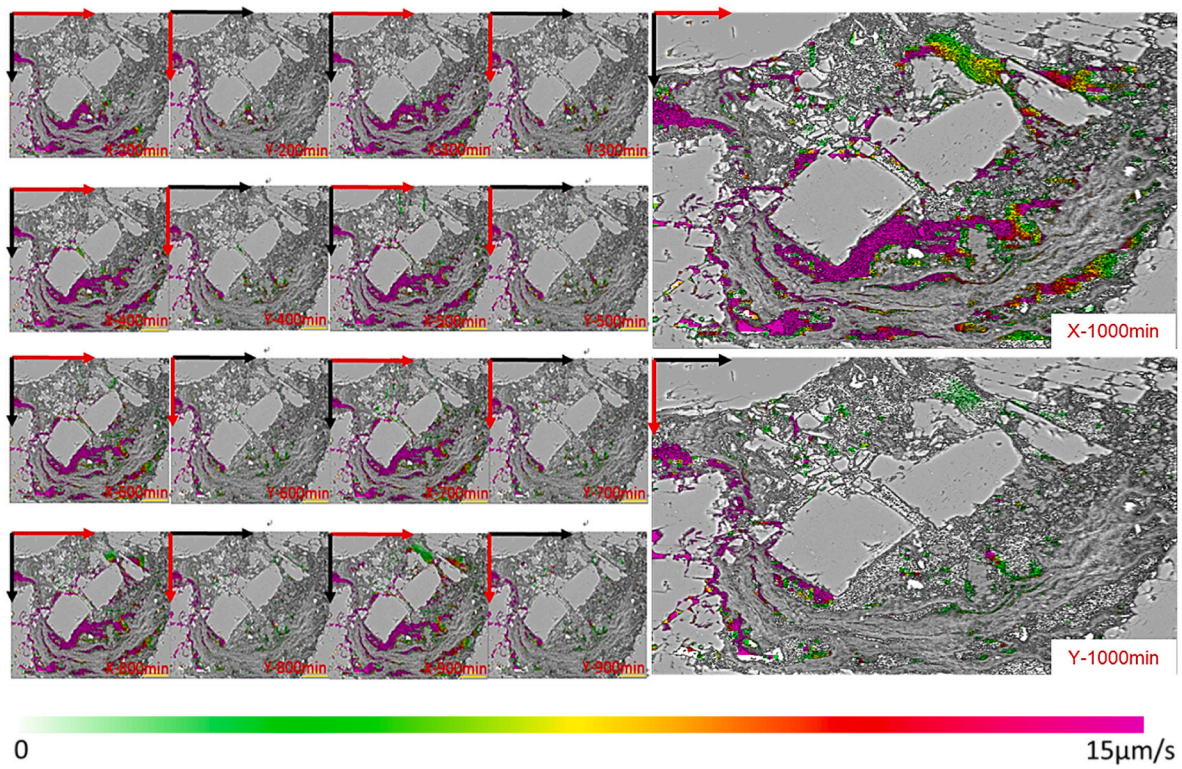

Fig. 12. Visual flow simulation of tight oil exploitation (200–1000min). The final flow state is shown in the X–velocity (horizontal velocity) and Y–velocity (vertical velocity) in 1000 min.

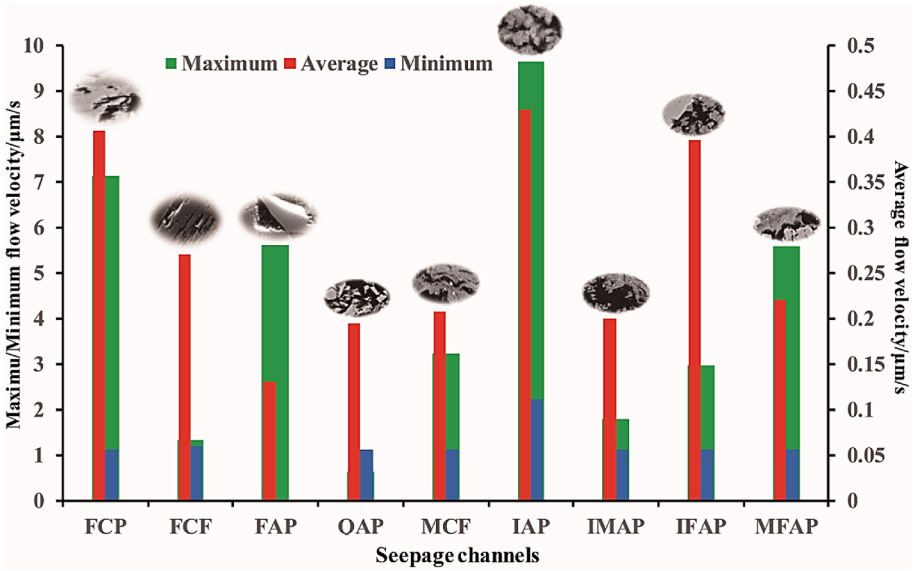

Fig. 13. Flow velocity distribution of each type of space in the seepage channels.

In equation (6), F indicates the fractal dimension, R indicates the box radius, and N_r indicates the number of boxes contained in the image under the relative box radius.

As seen in Fig. 8 ~10, the fractal dimension, the contents and the average diameters of seepage channels are all varied in seepage channels formed by various minerals.

In Fig. 8, the rank of the fractal dimension is accumulational pore of the interstitial fillings-black mica (IMAP), corrosional pore inside the feldspar (FCP), accumulational pore of the interstitial fillings-feldspar (IFAP), accumulational pore by the quartz broken (QAP), accumulational pore of the black mica-feldspar (MFAP), corrosional fracture inside the feldspar (FCF), accumulational pore of the interstitial fillings (IAP), fracture inside the black mica cleavage (MCF), and accumulational pore caused by the feldspar broken (FAP).

As the fractal dimension indicates the complexity of the seepage channels, the higher the value, the more complex the seepage channel is. The accumulational pore of the interstitial fillings–black mica (IMAP) and the accumulational pore by the feldspar broken (FAP) occupied the maximum and minimum of the fractal dimension respectively.

As seen in Fig. 9, the rank of the seepage channels content is IAP,

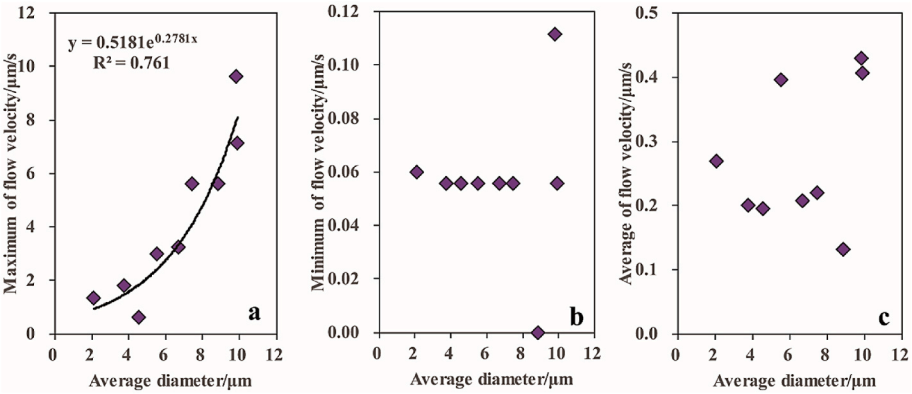

Fig. 14. Cross–plot of average diameter and the flow velocity. Each point indicates the properties of a type of seepage channel. The black curve is the fitting curve which could show that there is a satisfied binomial relationship between average diameter and the maximum of flow velocity.

FCP, IFAP, FAP, MFAP, MCF, QAP, FCF, and IMAP. As the content represents the probability of the porosity being affected throughout the entire flow process, the differences in the content of the seepage channels will have a different impact on the flow. The acumulational pore of the interstitial fillings (IAP) has the highest content while the corrosional fracture inside the feldspar (FCF) and the accumulational pore by the quartz broken (QAP) have the lowest content.

Similarly, as seen in Fig. 10, the rank of the average diameter is FAP, MFAP, IAP, MCF, IFAP, FCP, QAP, IMAP, FCF. As the average radius represents the space size of the fluid throughout the entire flow process, the differences in the radii of the seepage channels also represents the differences in the flow line form, which will have a different impact on the flow. The accumulational pore by the feldspar broken (FAP) has the highest value while the corrosional fracture inside the feldspar (FCF) has the lowest value.

3.3. Flow simulation results

As seen from Figs. 11 and 12, when we injected the injective liquid into a stationary location, the microscopic flow path had some regularities, which needed to be addressed. Throughout the entire flow process, the flow of the fluid in the nine seepage channels generally presents the characteristics of the earlier stage (0–200 min) and the later uniform propulsion (200 min–1000 min). As the flow process continues to advance, the diversity of the seepage channels begins to manifest gradually. The characteristics of the flow begin to appear to be uniform, but the flow characteristics in the different seepage channels are also very different, so it is worth studying this further.

In addition, the flow process in the horizontal direction (X direction) and the vertical direction (Y direction) is very different. Overall, the X direction is the dominant direction of the flow, and its flow rate is higher than the Y direction. This finding can be supported by evidence related to seepage channel extension (Figs. 11 and 12).

The vector modulation of the flow velocity in the X and Y directions was determined. When the simulation results of the two samples are combined, the statistics for the maximum, average, and minimum flow velocity for each type of seepage channels were also obtained (Fig. 12).

As to the maximum flow velocity, the rank is IAP, FCP, MFAP, FAP, MCF, IFAP, IMAP, FCF, and QAP. The acumulational pore of the interstitial fillings (IAP) has the highest value while the accumulational pore by the quartz broken (QAP) have the lowest (Fig. 13).

As to the minimum flow velocity, the rank is IAP, FCF, FCP, IFAP, QAP, IMAP, MCF, MFAP, and FAP. The acumulational pore of the interstitial fillings (IAP) has the highest value while the accumulational pore by the feldspar broken (FAP) have the lowest (Fig. 13).

As to the average flow velocity, the rank is IAP, FCP, IFAP, FCF, MFAP, MCF, IMAP, QAP, and FAP. The acumulational pore of the interstitial fillings (IAP) has the highest value while the corrosional fracture inside the feldspar (FCF) and the accumulational pore by the feldspar broken (FAP) have the lowest (Fig. 13).

The maximum flow velocity is shown on the left vertical axis while the average and minimum flow velocities are shown on the right vertical axis. The images of each type of seepage channels are shown in the column respectively.

4. Discussion

4.1. Mechanism of the differences in flow velocity and sweep efficiency

As seen in Fig. 14, the maximum of flow velocity increased for the non–linear flow as the average diameter of each type of space increased. Thus, the larger the diameter of the space, the greater the potential flow capability. This proves that as the injection pressure increases, the flow velocity could be higher in the larger seepage channels than in the smaller seepage channels.

The minimum flow velocity for each type of space is similar; most of the values remain at about 0.05 μm/s, which shows that the lowest potential flow capability has almost nothing to do with the type of space. This means that as long as the flow process occurs in the space, the lowest velocity is nearly the same (Fig. 14).

Similarly, the average flow velocity (the comprehensive potential flow capability) has almost no relationship with the type of space. This means that a small space does not have a higher potential of exploitation than a large space. It also demonstrates that our exploitation objective should not be primarily restricted to nanoscale spaces, such as gas contained in shale. The large space in a conventional reservoir could also have higher exploitation potential, so technology is needed to enhance the efficiency of microscopic oil displacement (Fig. 14).

In order to explore whether the geometric characteristics of 9 types of reservoir spaces will affect the flow velocity, four types of geometry attributes include “circularity”, “aspect ratio”, “roundness” and “solidity” were constructed and calculated respectively (Zeng et al., 2020). The correlation between these four types of geometry attributes and flow characteristics were also analyzed.

Their definition formulas are as follows,

$$Circularity = 4\pi \frac{Area}{perimeter^2} \tag{7}$$

$$Aspect\ Ratio = \frac{Major\ axis}{Minor\ axis} \tag{8}$$

$$Roundness = 4\frac{Area}{\pi * Major\ axis^2} \tag{9}$$

$$Solidity = \frac{Area}{Convex\ area} \tag{10}$$

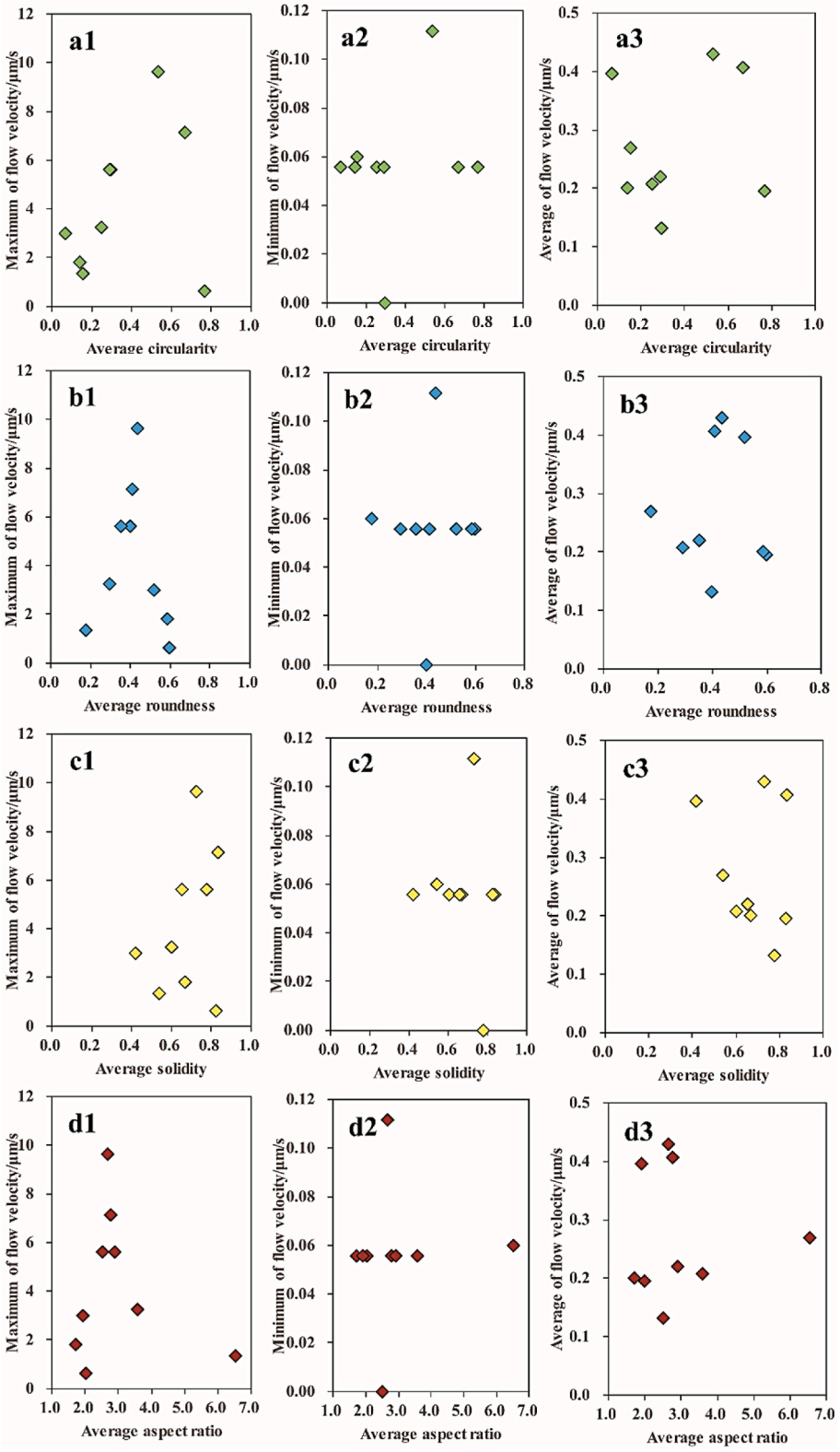

Fig. 15. Cross–plot of average circularity, roundness, solidity, aspect ratio and the maximum (a1, b1, c1, and d1), minimum (a2, b2, c2, and d2) and average (a3, b3, c3, and d3) of flow velocity. Each point indicates the properties of a type of seepage channel. Among them, "circularity" and "roundness" represent the degree of the reservoir space approaching the circle. The larger their values are, the closer they are to the circle. On the contrary, the greater the ovality is. "Aspect ratio" refers to the ratio of the length of the major axis to the minor axis after ellipse fitting of the boundary shape of the reservoir space. Solidity represents the concave and convex degree of the boundary of reservoir space. The smaller its value is, the more obvious the boundary is concave inward.

It can be seen from Fig. 15 that the average values of circularity, roundness, aspect ratio do not have obvious relationships with flow velocity. This proves that there is no strict quantitative relationship between the geometric parameters of single reservoir space and the flow velocity. In addition, the factors affecting the flow process are relatively complex, which may be caused by the change of the pore geometry in the reservoir space during the flow process.

To evaluate the sweep efficiency, the simulation results presented in Figs. 11 and 12 were combined, and the microscopic sweep efficiency index E_v was constructed as Equation (11).

$$E_v = \frac{N_i}{N} \tag{11}$$

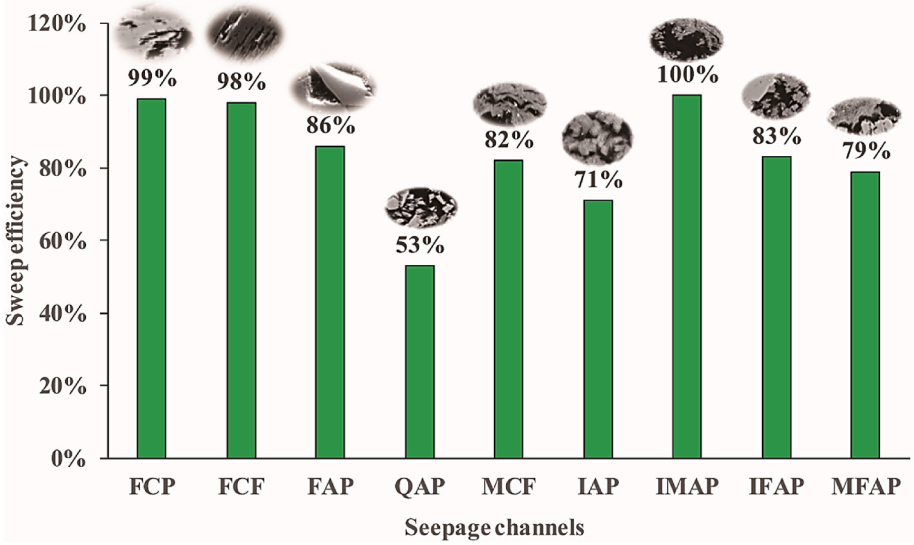

Fig. 16. The sweep efficiency distribution of each type of space in the seepage channels. The images of each type of seepage channels are shown in the column respectively.

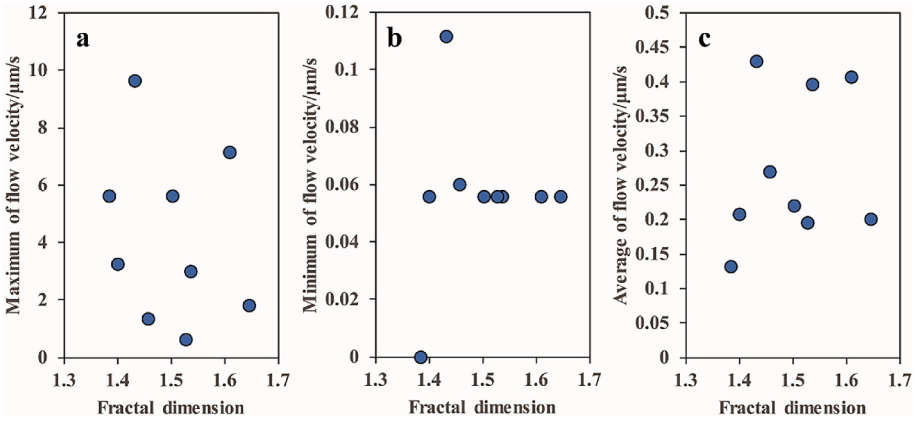

Fig. 17. Cross–plot between the fractal dimension and the maximum (a), minimum (b) and average (c) of flow velocity.

where N_i indicates that the number of grids whose velocity value is non–zero in each type of space at one time and N indicates the total number of grids that symbolize each type of space.

The microscopic sweep efficiency index of nine types of space in the seepage channels was also calculated (Fig. 16). The sequence is IMAP, FCP, FCF, FAP, IFAP, MCFH, MFAP, IAP, and QAP, which means that the potential of the residual oil in the accumulational pore by the quartz broken (QAP) and the accumulational pore of the interstitial fillings–-black mica (IMAP) would be the highest and lowest. This finding would also benefit the tight oil exploitation.

Obviously, the physical meaning in Formula (11) represents the extent to which different types of seepage channels are affected in the whole oil displacement process. This is one of the leading factors for the oil recovery efficiency in each type of seepage channels.

In addition, the combination of Figs. 13 and 16 is of great significance for the development of remaining oil. It clearly points out that the remaining oil may remain in the seepage channel with which mineral as the boundary, which has direct guidance for us to select the chemical materials for oil displacement or determine displacement pressure.

4.2. Relationship between the fractal dimension and the flowing characteristics

As we know, fractal dimension can reflect the structural complexity of different seepage channels (Du et al., 2018a, 2018b). However, whether the fractal dimension can reflect the flow velocity characteristics of different seepage channels is a topic worthy of discussion. So the cross–plot between the fractal dimension and the maximum (a), minimum (b) and average (c) of flow velocity were drawn (Fig. 17).

Fig. 17 shows that the relationship between the fractal dimension and the maximum, minimum and average flow velocity of different seepage channels is not particularly obvious, that is to say, the fractal dimension could not reflect the differences of flow velocity well. The possible mechanism is that although fractal dimension can reflect the complexity of porous media structure, there are many factors influencing the flow process in tight reservoir, and the weight of each factor is different, but it can be concluded that fractal dimension is not the most important one. Of course, the specific mechanism still needs further study.

4.3. Significance in tight oil exploitation

As to the mechanism of the differences in the flow process for

seepage channels formed by different minerals in a tight reservoir, we could illustrate it in the aspect of energy conversion. When the external fluid passes through the seepage channel, it is bound to be facing the boundary. From the point of view of energy conversion, there is a dynamic conversion of kinetic and elastic energy when fluid passes through the seepage channels formed by different minerals. Because different minerals have different elastic properties (Young's modulus, Poisson's ratio, Lame coefficient, etc.), the size and speed of these two types of energy conversions will vary greatly in the flow process. When the fluid flows through the seepage channels, if the mineral stiffness on the boundary is small (i.e., the Young's modulus is small), the kinetic energy of the fluid is easily converted to elastic energy. When the fluid leaves the seepage channel, the mineral is quickly recovered due to elastic energy, but the fluid cannot be converted to kinetic energy, thus resulting in energy loss. Conversely, if the mineral stiffness of the boundary is larger (i.e., the Young's modulus is large), the kinetic energy of the fluid is not easily converted to elastic energy, so the fluid energy loss is small and there is little variation in the flow velocity.

It should be pointed out that, the types of minerals that form different seepage channels are complex, and minerals have various wettabilities. So the tight oil reservoirs in this study behave as mixed-wet, which leads to the particularity of this type of tight oil reservoirs compared with reservoirs in other regions in terms of displacement efficiency and residual oil distribution characteristics. This also reflects the necessity and significance of conducting the study from the perspective of combining mineral types with seepage channels. It could be concluded that, in the middle and later periods of the oil exploitation, some oil may still remain in the large space. Therefore, it is not factual that the remaining oil is primarily found in the small seepage channels after water-flooding exploitation. It is reasonable to speculate that the oil was exploited from both the large and small space. However, sometimes, it could primarily be exploited from the large space.

5. Conclusions

The new seepage channels classification scheme was developed based on mineral types after considering the differences in their mechanical properties. The new classification scheme could be used to explore the influence of reservoir space types constructed by different mineral combinations on the flow process and potential of tight oil reservoirs. The different seepage channels formed by many types of minerals are varied in fractal dimension, contents, and average pore diameters.

Throughout the entire flow process, the diversity of the seepage channels begin to manifest gradually. The characteristics of the flow begin to appear to be uniform, but the flow characteristics in the different seepage channels are also very different, so it is worth studying this further. The larger the diameter of the space, the greater the potential flow capability. This could prove that as the injection pressure increases, the flow velocity could be higher in the larger seepage channels than in the smaller seepage channels.

The lowest potential flow capability has almost nothing to do with the type of seepage channel. This means that as long as the flow process occurs in the seepage channel, the lowest velocity is nearly the same.

As to the geometric properties of reservoir spaces, the average values of circularity, roundness, aspect ratio do not have obvious relationships with flow velocity. This proves that there is no strict quantitative relationship between the geometric parameters of single reservoir space and the flow velocity. In addition, the factors affecting the flow process are relatively complex, which may be caused by the change of the pore geometry in the reservoir space during the flow process.

Our exploitation objective should not be primarily restricted to nanoscale spaces, such as gas contained in shale. The large space in a conventional reservoir could also have higher exploitation potential, so technology is needed to enhance the efficiency of microscopic oil displacement.

It is reasonable to speculate that the oil was exploited from both the large and small seepage channel However, sometimes, it could primarily be exploited from the seepage channel.

Declaration of competing interest

The authors declare that they have no known competing financial interests or personal relationships that could have appeared to influence the work reported in this paper.

Data availability

Data will be made available on request.

Acknowledgements

This work was supported by PetroChina Innovation Foundation (Grant No.2019D-5007-0214).

References

Ahrens, T.J., 1995. Mineral Physics and Crystallography: a Handbook of Physical Constants. American Geophysical Union.

Alarji, H., Clark, S., Regenauer-Lieb, K., 2022. Wormholes effect in carbonate acid enhanced oil recovery methods. Adv. Geo-Energy Res. 6 (6), 492–501. https://doi.org/10.46690/ager.2022.06.06.

Alexandre, P., 2009. Mineralogy and geochemistry of the sodium- metasomatism related uranium occurrence of Aricheng South, Guyana. Miner. Deposita 45 (4), 351–367. https://doi.org/10.1007/s00126-010-0278-7.

Antoine, M., Cupillard, P., Giot, R., Conin, M., Leroy, Y., Thore, P., 2018. Stress estimation in reservoirs using an integrated inverse method. Comput. Geosci. 114, 30–40. https://doi.org/10.1016/j.cageo.2018.01.004.

Arash, K., Kc, B., Foroutan, M., Ghazanfari, E., Cladouhos, T.T., Stevens, M., 2019. Stress-strain response and seismic signature analysis of phyllite reservoir rocks from Blue Mountain geothermal field. Geothermics 77. https://doi.org/10.1016/j.geothermics.2018.09.004.

Babiak, M., Gaff, M., Sikora, A., Hysek, Š., 2018. Modulus of elasticity in three-and four-point bending of wood. Compos. Struct. 204, 454–465. https://doi.org/10.1016/j.compstruct.2018.07.113.

Benito, J.A., Jorba, J., Manero, J.M., Roca, A., 2005. Change of Young's modulus of cold-deformed pure iron in a tensile test. Metall. Mater. Trans. 36 (12), 3317–3324. https://doi.org/10.1007/s11661-005-0006-6.

Cabalar, A.F., Khalaf, M.M., Karabash, Z., 2018. Shear modulus of clay-sand mixtures using bender element test. Acta Geotechnica Slovenica 15 (1), 3–15. https://doi.org/10.18690/actageotechslov.15.1.3-15.2018.

Cai, J.C., Zhao, L.X., Zhang, F., Wei, W., 2022. Advances in multiscale rock physics for unconventional reservoirs. Adv. Geo-Energy Res. 6 (4), 271–275. https://doi.org/10.46690/ager.2022.04.01.

Cao, H.S., Kaufman, J. Alan, Shan, X.L., 2016a. Sulfur isotope constraints on marine transgression in the lacustrine Upper Cretaceous Songliao Basin, northeastern China. Palaeogeogr. Palaeoclimatol. Palaeoecol. 451, 152–163. https://doi.org/10.1016/j.palaeo.2016.02.041.

Cao, Z., Liu, G.D., Zhan, H.B., Li, C.Z., You, Y., Yang, C.Y., Jiang, H., 2016b. Pore structure characterization of Chang–7 tight sandstone using MICP combined with N2 GA techniques and its geological control factors. Sci. Rep. 6, 36919 https://doi.org/10.1038/srep36919.

Du, S.H., Shi, Y.M., Bu, X.Q., Jin, W.Q., Mu, G.Q., 2015. New expression of the changing stress field in low-permeability reservoir and its application in secondary exploitation. Energy Explor. Exploit. 33, 491–514. https://doi.org/10.1260/0144-5987.33.4.491.

Du, S.H., Shi, Y.M., Guan, P., Zhang, Y.G., 2016. New inspiration on effective development of tight reservoir in secondary exploitation by using rock mechanics method. Energy Explor. Exploit. 34, 3–18. https://doi.org/10.1177/0144598715623661.

Du, S.H., Pang, S., Shi, Y.M., 2018a. A new and more precise experiment m-ethod for characterizing the mineralogical heterogeneity of unconventional hydrocarbon reservoirs. Fuel 232, 666–671. https://doi.org/10.1016/j.fu-el.2018.06.012.

Du, S.H., Pang, S., Shi, Y.M., 2018b. Quantitative characterization on the microscopic pore heterogeneity of tight oil sandstone reservoir by considering both the resolution and representativeness. J. Petrol. Sci. Eng. 169, 388–392. https://doi.org/10.1016/j.petrol.2018.05.058.

Du, S.H., Xu, F., Abitkazy, T., Zhou, B., Kou, G., Shi, Y.M., 2019a. Anisotropy characteristics of element composition in Upper Triassic "Chang 8" shale in Jiyuan district of Ordos Basin, China: microscopic evidence for the existence of predominant fracture zone. Fuel 253, 685–690. https://doi.org/10.1016/j.fuel.2019.05.031.

Du, S.H., Zhao, Y.P., Jin, J., Kou, G., Shi, Y.M., Huang, X.F., 2019b. Significance of the secondary pores in perthite for oil storage and flow in tight sandstone reservoir. Mar. Petrol. Geol. 110, 178–188. https://doi.org/10.1016/j.marpetgeo.2019.07.006.

Du, S.H., Shi, Y.M., Zheng, X.J., Chai, G.S., 2020. Using "Umbrella Deconstruction & Energy Dispersive Spectrometer (UD-EDS)" technique to quantify the anisotropic

elements distribution of" Chang 7" shale and its significance. Energy 191, 116443. https://doi.org/10.1016/j.energy.2019.116443.
Eremin, M., Esterhuizen, G., Smolin, I., 2020. Numerical simulation of roof cavings in several Kuzbass mines using finite-difference continuum damage mechanics approach. Int. J. Min. Sci. Technol. 30 (2), 157–166. https://doi.org/10.1016/j.ijmst.2020.01.006.
Ge, X.M., Fan, Y.R., Li, J.T., Zahid, M.A., 2015. Pore structure characterization and classification using multifractal theory—an application in Santanghu basin of western China. J. Petrol. Sci. Eng. 127, 297–304. https://doi.org/10.1016/j.petrol.2015.01.004.
Ge, X.M., Fan, Y.R., Xiao, Y.F., Liu, J.Y., Xing, D.H., Gu, D.N., Deng, S.G., 2017. Quantitative evaluation of the heterogeneity for tight sand based on the nuclear magnetic resonance imaging. J. Nat. Gas Sci. Eng. 38, 74–80. https://doi.org/10.1016/j.jngse.2016.12.037.
Geng, X.Z., 2020. A new wellbore fluid load diagnosing model based on the energy conservation law. Nat. Gas. Ind. B 7 (2), 141–148. https://doi.org/10.1016/j.ngib.2019.09.002.
Gran, K., Paola, C., 2001. Riparian vegetation controls on braided stream dynamics. Water Resour. Res. 37 (12), 3275–3283. https://doi.org/10.1029/2000WR000203.
Gula, J., Molemaker, M.J., McWilliams, J.C., 2015. Gulf Stream dynamics along the southeastern US seaboard. J. Phys. Oceanogr. 45 (3), 690–715. https://doi.org/10.1175/JPO-D-14-0154.1.
Guo, X.W., Shi, Y.M., Yang, Y., Chai, Z., Wu, L.F., 2013. Analysis of the influencing factors of the tight reservoirs of oil group Chang-6 in Ordos basin. Pet. Geol. Oilfield Dev. Daqing 32 (5), 165–169. https://doi.org/10.3969/J.ISSN.1000-3754.2013.05.034.
Hematpur, H., Abdollahi, R., Rostami, S., Haghighi, M., Blunt, M.J., 2023. Review of underground hydrogen storage: Concepts and challenges. Adv. Geo-Energy Res. 7 (2), 111–131. https://doi.org/10.46690/ager.2023.02.05.
Hou, B.F., Wang, Y.F., Cao, X.L., 2015. Mechanisms of enhanced oil recovery by surfactant–induced wettability alteration. J. Dispersion Sci. Technol. 37, 1259–16267. https://doi.org/10.1080/01932691.2015.1089778.
Hu, Y., Li, X.Z., Wan, Y.J., Lu, J.L., Zhu, H.Y., Zhang, Y.F., Zhu, Q.Y., Ya-ng, M., Niu, L. W., 2013. Physical simulation on gas flow in tight s-andstone: Petrol. Explor. Dev. 40, 580–584. https://doi.org/10.11698/PED.2013.05.10.
Hu, J.H., Yang, S.G., Fu, D.M., Rui, R., Yu, Y.L., Chen, Z.X., 2016. Rock mechanics of shear rupture in shale gas reservoirs. J. Nat. Gas Sci. Eng. 36, 943–949. https://doi.org/10.1016/j.jngse.2016.11.033.
Hu, J.H., Zhang, C., Rui, Z.H., Yu, Y.L., Chen, Z.X., 2017. Fractured horizontal well productivity prediction in tight oil reservoirs. J. Petrol. Sci. Eng. 151, 159–168. https://doi.org/10.1016/j.petrol.2016.12.037.
Huang, W.B., Lu, S.F., Hersi, O.S., Wang, M. Deng, Lu, S.W., Jing, R., 2017. Reservoir spaces in tight sandstones: classification, fractal characters, and heterogeneity. J. Nat. Gas Sci. Eng. 46, 80–92. https://doi.org/10.1016/j.jngse.2017.07.006.
Jiang, F.J., Chen, D., Wang, Z.F., 2016. Pore characteristic analysis of a lacustrine shale: a case study in the Ordos Basin, NW China. Mar. Petrol. Geol. 73, 554–571. https://doi.org/10.1016/j.marpetgeo.03.026.
Ju, W., Shen, J., Qin, Y., Meng, S.Z., Wu, C.F., Shen, Y.L., Yang, Z.B., Li, G.Z., Li, C., 2017. In–situ stress state in the Linxing region, eastern Ordos Basin, China: implications for unconventional gas exploration and production. Mar. Petrol. Geol. 86, 66–78. https://doi.org/10.1016/j.marpetgeo.2017.05.026.
Kang, Y.L., Tu, Y.Q., You, L.J., Li, X.C., Huang, F.S., 2019. An experimental study on oxidizer treatment used to improve the flow capacity of coal reservoirs. Nat. Gas. Ind. B 6 (2), 129–137. https://doi.org/10.1016/j.ngib.2018.09.003.
Krohnce, 1988. Sandstone fractal and euclidean pore volume distributions. J. Geophys. Res. 93 (B4), 3297–3305.
Lager, A., Webb, K.J., Black, C.J.J., 2007. Impact of Brine Chemistry on Oil Recovery: Paper A24 Presented at the 14th European Symposium on Improved Oil Recovery. Cairo, Egypt, 22–24 April.
Li, Z.L., 2015. An augmented Cartesian grid method for Stokes–Darcy fluid–structure interactions. Nternational Journal for Numerical Methods in Engineering 106, 556–575. https://doi.org/10.1002/nme.5131.
Li, C.L., Zhang, X.L., 2007. Unification of flow equations in tubes and in porous media. Xinjing Pet. Geol. 28 (2), 252–253.
Liang, J.Y., Jia, G.Z., 2022. China futures price forecasting based on online search and information transfer. Data Sci. Manag. 5 (4), 187–198. https://doi.org/10.1016/j.dsm.2022.09.002.
Ligthelm, D.J., Gronsveld, J., Hofman, J.P., Brussee, N.J., Marcelis, F., van der Linde, H. A., 2009. Novel Waterflooding Strategy by Manipulation of Injection Brine Composition: Paper SPE 119835 Presented at the 2009 SPE EUROPEC/EAGE Annual Conference and Exhibition. Amsterdam, The Netherlands, 8–11 June.
Liu, J.Y., Ai, S.Z., Du, R., Brugha, C.M., 2022. Analysis of commodity traceability service effects on the purchase behavior of consumers using an evolutionary game model. Data Sci. Manag. 5 (4), 175–186. https://doi.org/10.1016/j.dsm.2022.08.003.
Macquaker, J.H.S., Taylor, K.G., Keller, M., 2014. Compositional controls on early diagenetic pathways in fine–grained sedimentary rocks: implications for predicting unconventional reservoir attributes of mudstones. AAPG (Am. Assoc. Pet. Geol.) Bull. 93, 587–603. https://doi.org/10.1306/08201311176.
Mandelbrot, B.B., 1967. How long is the coast of Britain? Statistical self-similarity and fractional dimension. Science 156 (3775), 636–638. https://doi.org/10.1126/science.156.3775.636.
Mandelbrot, B.B., 1974. Intermittent turbulence in self-similar cascades: divergence of high moments and dimension of the carrier. J. Fluid Mech. 62 (2), 331–358. https://doi.org/10.1017/S0022112074000711.
Markevich, N.J., Ceil, I., 1991. Through Flow Analysis for Rockfill Dam Stability Evaluations: Waterpower: A New View of Hydro Resources, pp. 1734–1743.
Mathew, T.V., Natarajan, S., Martínez-Pañeda, E., 2018. Size effects in elastic-plastic functionally graded materials. Compos. Struct. 204, 43–51. https://doi.org/10.1016/j.compstruct.2018.07.048.
Nishank, S., Hofmann, R., Alpak, F.O., 2017. References and benchmarks for pore–scale flow simulated using micro–CT images of porous media a-nd digital rocks. Adv. Water Resour. 109, 211–235. https://doi.org/10.1016/j.advwatres.2017.09.007.
Nittman, J., 1985. Fractal growth of viscous fingers: quantitative characterization of a fluid instability phenomenon. Nature 314, 141–144.
Nurudeen, Y., Padmanabhan, E., Idris, A.K., 2018. A review of recent advances in foam-based fracturing fluid application in unconventional reservoirs. J. Ind. Eng. Chem. 66, 45–71. https://doi.org/10.1016/j.jiec.2018.05.039.
Peng, R.D., Yang, Y.C., Ju, Y., Mao, L.T., Yang, Y.M., 2011. Computation of fractal dimension of rock pores based on gray CT images. Chin. Sci. Bull. 56 (31), 3346. https://doi.org/10.1007/s11434–011–4683–9.
Pia, G., Cristina, S., Ludovica, C., 2016. Pore size distribution and porosity influence on sorptivity of ceramic tiles: from experimental data to fractal modelling. Ceram. Int. 42 (8), 9583–9590. https://doi.org/10.1016/j.ceramint.2016.03.041 do-i:
Sakran, S., Muhammad, N., Ahmed, H., 2015. Structural regime and its imp-act on the mechanism and migration pathways of hydrocarbon flow in the southern Gulf of Suez rift: an approach for finding new unex-plored fault blocks. Mar. Petrol. Geol. 71, 55–75. https://doi.org/10.1016/j.marpetgeo.2015.12.003 d-oi:
Sakran, S., Muhammad, N., Ahmed, H., 2016. Fracture reopening by micro–earthquakes, a mechanism for oil flow in mildly active rifts: a case study from Gemsa oilfield, the southern Gulf of Suez rift, Egypt. Arabian J. Geosci. 9, 404. https://doi.org/10.1007/s12517-016-2433-7.
Salem, A.M., 2005. Agenesis and reservoir–quality evolution of incised–valley sandstones: evidence from the abu madi gas reservoirs (upper miocene), the nile delta basin. J. Sediment. Res. 75 (4), 572–584. https://doi.org/10.2110/jsr.2005.047.
Stokes, C.R., Clark, C.D., Storrar, R., 2009. Major changes in ice stream dynamics during deglaciation of the north-western margin of the Laurentide Ice Sheet. Quat. Sci. Rev. 28 (7–8), 721–738. https://doi.org/10.1016/j.quascirev.2008.07.019.
Strand, S., Puntervold, T., Austad, T., 2016. Water based EOR from clastic oil reservoirs by wettability alteration: a review of chemical aspects. J. Petrol. Sci. Eng. 146, 1079–1091. https://doi.org/10.1016/j.petrol.2016.08.012.
Tan, Q.G., You, L.J., Kang, Y.L., Zhang, X.W., Meng, S., 2020. Changes in pore structures and porosity-permeability evolution of saline-lacustrine carbonate reservoir triggered by fresh water-rock reaction. J. Hydrol. 580, 124375 https://doi.org/10.1016/j.jhydrol.2019.124375.
Tozzi, L., Laurent, P.A., Di Buduo, C.A., Mu, X., Massaro, A., Bretherton, R., Stoppela, W., Kaplan, D.L., Balduini, A., 2018. Multi-channel silk sponge mimicking bone marrow vascular niche for platelet production. Biomaterials 178, 122–133. https://doi.org/10.1016/j.biomaterials.2018.06.018.
Wan, Y.W., Zhang, H., Liu, X.J., Yin, G.Q., Xiong, J., Liang, L.X., 2020. Prediction of mechanical parameters for low-permeability gas reservoirs in the Tazhong Block and its applications. Adv. Geo-Energy Res. 4 (2), 219–228. https://doi.org/10.26804/ager.2020.02.10.
Wang, F., Li, Y., Tang, X., Chen, J., Gao, W., 2016a. Petrophysical properties analysis of a carbonate reservoir with natural fractures and vugs using X–ray computed tomography. J. Nat. Gas Sci. Eng. 28, 215–225. https://doi.org/10.1016/j.jngse.2015.11.046.
Wang, J.M., Guo, L.L., Bai, Z.K., 2016b. Using computed tomography (CT) images and multi–fractal theory to quantify the pore distribution of reconstructed soils during ecological restoration in opencast coal–mine. Ecol. Eng. 92, 148–157. https://doi.org/10.1016/j.ecoleng.2016.03.029.
Wang, S.Y., 2021. An interview with Shouyang Wang: research frontier of big data-driven economic and financial forecasting. Data Sci. Manag. 1 (1), 10–12. https://doi.org/10.1016/j.dsm.2021.01.001.
Xu, C.F., Liu, H.X., Qian, G.B., Qin, J.H., 2011. Microcosmic mechanism-s of water–oil displacement in conglomerate reservoirs in Karamay Oil-field, NW China. Petrol. Explor. Dev. 38 (6), 725–732. https://doi.org/10.1016/S1876-3804(12)60006-8.
Xu, L., 2017. Quantitative characterization and different formation mechanism of secondary pores of tight sandstone reservoirs. Ph.D. thesis. Peking University, Beijing, pp. 1–95 (in Chinese with English abstract).
Xu, Z.B., Tang, N.S., Xu, C., Cheng, X.Q., 2021. Data science: connotation, methods, technologies, and development. Data Sci. Manag. 1 (1), 32–37. https://doi.org/10.1016/j.dsm.2021.02.002.
Yuan, W.F., 2020. Water-sensitive characterization and its controlling factors in clastic reservoir: a case study of Jurassic Ahe Formation in Northern tectonic zone of Kuqa depression. Petroleum Research 5 (1), 77–82. https://doi.org/10.1016/j.ptlrs.2019.07.002.
Zeng, Y.J., Du, S.H., Zhang, X., Zhang, B.P., Liu, H.L., 2020. The crucial geometric distinctions of microfractures as the indispensable transportation channels in hydrocarbon-rich shale reservoir. Energy Rep. 6, 2056–2065. https://doi.org/10.1016/j.egyr.2020.07.004.
Zhang, B., Yan, S.Y., Gu, Z.D., Zhang, J.J., 2013. SEM/EBSD analysis of quartz cementation and compaction microstructures during diagenesis of sandstone. Sci. China Earth Sci. 56 (8), 1281–2129-3. https://doi.org/10.1007/s11430–013–4612–7.
Zhao, Y.P., 2018. Lectures on Mechanics. Science Press, Beijing, pp. 351–356.

Zhao, X., Yang, Z., Lin, W., Xiong, S., Luo, Y., Liu, X., Xia, D., 2019. Fractal study on pore structure of tight sandstone based on full-scale map. Int. J. Oil Gas Coal Technol. 22 (2), 123–139.

Zhu, Q., Che, J.H., Li, Y.Z., Zuo, R.X., 2022. A new prediction nn framework design for individual stock based on the industry environment. Data Sci. Manag. 5 (4), 199–211. https://doi.org/10.1016/j.dsm.2022.09.001.

Zhu, W.Y., Liu, Y.W., Shi, Y.Q., Zou, G.D., Zhang, Q.T., Kong, D.B., 2022. Effect of dynamic threshold pressure gradient on production performance in water-bearing tight gas reservoir. Adv. Geo-Energy Res. 6 (4), 286–295. https://doi.org/10.46690/ager.2022.04.03.